PHYSICAL REVIEW B **83**, 205120 (2011)

Magneto-optical and magnetoplasmonic properties of epitaxial and polycrystalline Au/Fe/Au trilayers

E. Ferreiro-Vila,[1] M. Iglesias,[2] E. Paz,[2] F. J. Palomares,[2] F. Cebollada,[3] J. M. González,[4] G. Armelles,[1] J. M. García-Martín,[1] and A. Cebollada[1]

[1]*IMM-Instituto de Microelectrónica de Madrid (CNM-CSIC), Isaac Newton 8, PTM,E-28760 Tres Cantos, Madrid, Spain*

[2]*Instituto de Ciencia de Materiales de Madrid (CSIC), Cantoblanco, E-28049 Madrid, Spain*

[3]*POEMMA, Departamento de Física Aplicada a las T.I., Universidad Politécnica de Madrid, E-28031 Madrid, Spain*

[4]*Unidad Asociada ICMM-CSIC/IMA-UCM, Sor Juana Inés de la Cruz 3, E-28049 Madrid, Spain*

(Received 15 March 2011; published 20 May 2011)

A complete study of the magneto-optical (MO) and magnetoplasmonic properties of both epitaxial and polycrystalline Au/Fe/Au multilayers as a function of Fe thickness is reported. An increase for both the MO activity without surface-plasmon-polariton (SPP) excitation and the magnetic modulation of the SPP wave vector for epitaxial structures compared to the polycrystalline ones is observed. This difference is related with the larger interface roughness of the polycrystalline structures that as a consequence, exhibit a reduction in the Fe MO constants. A comparative study of the MO activity with SPP excitation for both epitaxial and polycrystalline structures is also presented, being the key factor in the deposition of the adequate layer thickness to achieve optimum SPP excitation with independence of their crystalline nature.

DOI: 10.1103/PhysRevB.83.205120 PACS number(s): 78.20.Ls, 73.20.Mf, 78.66.Bz

I. INTRODUCTION AND MOTIVATION

Surface-plasmon polaritons (SPPs) are transversal electromagnetic waves bound to the interface between materials with dielectric constants of opposite signs.[1] Nowadays the properties of SPPs excited in different structures are being intensively investigated in view of their use in a number of applications that include nanophotonic circuits,[2–4] near-field scanning optical microscopy,[5,6] and biosensors.[7,8]

A crucial aspect for the advance of plasmonics is the development of active elements, i.e., systems whose plasmonic properties can be modified by an external agent. For that purpose, and in addition to the use of quantum dots[9] and thermo-optic[10] and electro-optic[11] materials, a promising approach is the incorporation of a ferromagnetic component into the plasmonic system, thus forming a magnetoplasmonic structure. In such structures, a great deal of intertwined plasmonic and magneto-optical (MO) phenomena has been studied.[12–22] To mention a few, the first studies were carried out in Au/Co/Au trilayers,[12,13] exploring the effect of SPP excitation in the MO properties. These studies were later extended, exploring the effect of the Co layer thickness.[14] There, the observed enhancement of the MO activity when SPP was excited was shown to be due to the combined action of the intense decrease of the reflectivity of the system and the enhanced electromagnetic field inside the MO active layer.[14] Subsequently, and due to the lower optical absorption of Ag compared to Au, Au/Ag/Co/Ag structures were also fabricated to study the relevance of the optical constants of the plasmonic material in these multilayers.[18]

However, a key but yet unexplored issue is the effect of both crystallinity (grain size or grain boundary scattering) and surface and interface roughness in the magnetic, optical, MO, and mainly magnetoplasmonic properties of these noble metal-ferromagnetic heterostructures. In fact, many previous works have shown that surface flatness,[23,24] grain size,[25–28] and epitaxial growth[29] play an important role in the optical constants of plasmonic nanostructures. On the other hand, different works indicate that the magnetic and MO properties of multilayered structures may also be affected by the morphology[30,31] and the interface flatness[32,33] of the ferromagnetic layer inside a heterostructure. Even polycrystalline Au/Fe/Au trilayers, used for biosensing purposes as a magneto-optical surface-plasmon resonance (MOSPR) sensor, exhibit lower MO performance than the expected ones,[34] probably due to the reduced MO properties of Fe in contact with Au. All these facts indicate that if the structural and morphological characteristics can strongly determine the MO constants of a magnetoplasmonic multilayered system, the MO activity and the magnetic modulation of the SPP wave vector, both dependent on the MO constants, would be strongly modified.

In this work we present a complete study on the influence of the magnetoplasmonic properties of the morphology, surface flatness, and epitaxial character of Au/Fe/Au multilayered structures grown on MgO substrates. The structure of the paper is as follows. Sec. II describes the experimental and theoretical methods used. Sec. III contains the complete characterization of the structures: Sec. III A describes their crystalline structure and morphology, Sec. III B is devoted to their magnetic properties, Sec. III C studies the MO properties, and Sec. III D analyzes the magnetoplasmonic behavior, including the modification of the MO activity upon SPP excitation and also the magnetic modulation of the SPP wave vector. Finally, Sec. IV summarizes the main conclusions.

II. EXPERIMENTAL AND THEORETICAL METHODS

Sample growth was performed under ultrahigh vacuum conditions in a system equipped with a combination of pulsed laser deposition (PLD) and molecular beam epitaxy (MBE) techniques. Two series of 7 nm Au/X nm Fe/7 nm Au structures, with Fe thickness varying between 0 and 6 nm, have been grown at room temperature (RT) on MgO(001) substrates. Buffer layers, namely, 1 nm Fe and 2 nm Cr, were

used to fabricate the otherwise equivalent series of samples. The Fe buffer layers were grown by PLD, whereas the Cr ones were grown by MBE. Fe layers were deposited by a Nd-YAG (yttrium aluminium garnet) laser ($\lambda = 532$ nm, 4 ns pulses, 25 mJ/pulse, 10 Hz repetition rate), and Au layers were also deposited by MBE. Prior to deposition, the MgO substrates were outgassed at 200 °C for 25 min for water desorption purposes and then cooled down to RT for thin-film deposition. Deposition rates were 1 nm/min for the Au and Cr layers and 0.5 nm/min for the Fe layers. The surface morphology of the fabricated structures was characterized by atomic force microscopy (AFM). AFM images were taken using a Nanotec™ microscope operating in noncontact dynamic mode, i.e., with a mechanically modulated cantilever. Silicon cantilevers from NanoSensors™ with a force constant $k = 5$ N/m and tip radius of 10 nm were used.

The crystallinity of all the samples was characterized by x-ray diffraction (XRD) using a Bragg-Brentano configuration and 1/4° slits. X-ray reflectivity (XRR) was used to determine layer thickness and interface roughness by the use of a parabolic mirror and a 0.27° parallel-plate collimator. XRD and XRR measurements were performed using Cu $K\alpha$ radiation ($\lambda = 1.5418$ Å).

Magnetic hysteresis loops at room temperature, with magnetic fields applied in-plane and out of plane, were obtained by Kerr measurements in transverse and polar configurations, respectively. The transverse Kerr loops were recorded by using a linearly polarized 532 nm light beam (solid-state laser) at 45° incidence angle geometry with the applied magnetic field in the film plane but perpendicular to the plane of incidence, and measuring the variations in the reflected light intensity. In the case of the polar Kerr loops, linearly polarized 600 nm light at normal incidence was used with the magnetic field applied perpendicularly to the film plane, and the Kerr rotation angle and the ellipticity of the elliptically polarized reflected light were measured.

Reflectivity (R) and transverse MO Kerr-effect ($\Delta R/R$) curves in the presence of plasmon excitation were also measured with a p-polarized HeNe laser and the sample mounted on a glass prism in Kretschmann configuration[35] to couple the wave vector of the incident light with that of the SPP. The magnitude $\Delta R/R$ is defined as

$$\frac{\Delta R}{R} \equiv \frac{R_{pp}(+H) - R_{pp}(-H)}{R_{pp}(+H) + R_{pp}(-H)}, \qquad (1)$$

where $R_{pp}(+H)$ and $R_{pp}(-H)$ stand for the reflectivity (both incident and reflected light being p polarized) for maximum positive and negative applied field, respectively. With this definition the maximum reachable value of $\Delta R/R$ is 1.

The different elements of the dielectric tensor of the system (diagonal or purely optical as well as nondiagonal or magneto-optical) were obtained via combined spectral ellipsometry and Kerr-effect measurements. Ellipsometry measurements were taken with a M200FI J. A. Woollam Co.™ ellipsometer between 500 nm and 1.69 μm, for angles of incidence ranging from 45° to 75°, which allowed the extraction of both real and imaginary parts (${\varepsilon^{xx}}_1$ and ${\varepsilon^{xx}}_2$, respectively) of the diagonal elements of the dielectric tensor. Polar Kerr spectra[36] were measured between 290 and 840 nm with a maximum magnetic field of 1.6 T. From the polar Kerr spectra, and knowing the diagonal elements of the dielectric tensor of the system, the real and imaginary parts of the nondiagonal elements (${\varepsilon^{xy}}_1$ and ${\varepsilon^{xy}}_2$, respectively) can be calculated. Since the Fe layers are cubic we can assume that the nondiagonal dielectric tensor elements are the same for all directions ($\varepsilon^{xy} = \varepsilon^{xz} = \varepsilon^{yz}$).

Simulations of the MO Kerr signal, with and without SPP excitation for such structures, were performed via a transfer-matrix method using the actual dielectric tensor elements of the materials obtained from ellipsometric and polar Kerr spectra.

III. RESULTS AND DISCUSSION

A. Structure and morphology

The crystalline structure of both series of samples, with Fe buffer layer grown by PLD and Cr buffer layer grown by MBE, has been studied by XRD. Fe and Cr are elements with body-centered cubic structures and very similar lattice parameters (0.287 and 0.288 nm, respectively). It is well known that both can grow epitaxially on MgO(001) substrates[37,38] upon 45° in-plane rotation of their crystalline lattice to match the 0.4213 nm lattice parameter of the substrate. Therefore they are both excellent candidates as a buffer layer to promote the epitaxial growth of a wide variety of metallic systems. However, we have found significant differences between the two series. Symmetric scans of samples with an Fe interlayer thickness of 6 nm are shown in Fig. 1(a). As can be seen, the growth

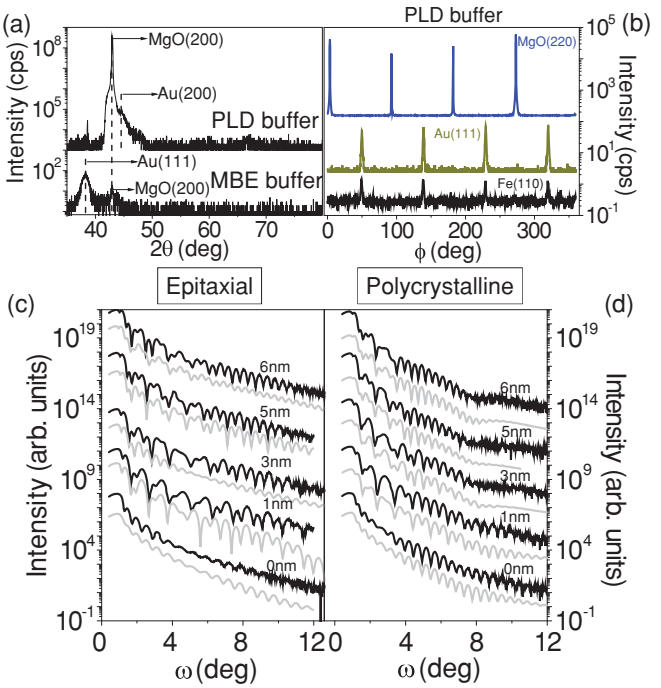

FIG. 1. (Color online) (a) High-angle symmetric x-ray diffraction scans for representative epitaxial and polycrystalline trilayers, respectively. (b) Phi scans of asymmetric reflections of MgO, Au, and Fe showing the epitaxial nature of the structures grown by PLD. X-ray reflectometry scans (black curves) together with best fits (gray curves) for the epitaxial (c) and polycrystalline (d) structures.

by PLD of an Fe buffer layer clearly promotes (001)-oriented growth along the out-of-plane direction, with the observation of Au(200) and MgO(200) diffraction peaks. The epitaxial nature of the PLD buffer sample is also confirmed by the asymmetric XRD ϕ scans shown in Fig. 1(b), where scans for MgO(220), Au(111), and Fe(110) diffraction peaks are shown. On the other hand, the samples with a Cr buffer layer grown by MBE exhibit a polycrystalline, textured growth, as shown by the Au (111) diffraction peak in Fig. 1(a).

Important differences have been obtained in XRR measurements and AFM analysis, which indicate that PLD deposition has a unique capability to produce ultraflat films due to the energy of the deposited atoms and the characteristic deposition rates.[39,40] In the bottom panel of Fig. 1, we show XRR curves and their corresponding best fits for both epitaxial and polycrystalline series of samples [Figs. 1(c) and 1(d), respectively]. The XRR curves of epitaxial structures show that the oscillations extinguish at higher 2θ angles compared to the polycrystalline structures due to the flatness of the interfaces in the epitaxial multilayers. In fact, the roughness analysis of the XRR curves fits values of 0.2 nm for the Au topmost layer in the epitaxial sample with a 6 nm Fe interlayer thickness as compared to 0.5 nm for the same Fe interlayer thickness in the polycrystalline structure.

Representative AFM images of the topmost surface of two samples without Fe interlayers and two other equivalent ones with Fe interlayers (4.5 and 5 nm of Fe interlayer thickness, respectively) for both the epitaxial and polycrystalline series

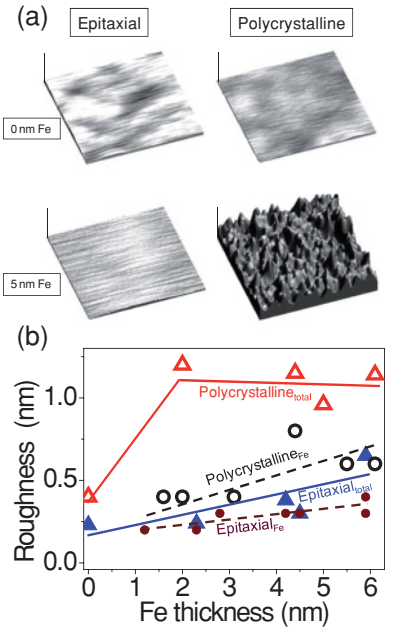

FIG. 2. (Color online) (a) AFM images for the two samples without an Fe interlayer and the two representative Fe interlayer samples (4.5 and 5 nm Fe thickness, respectively) for the epitaxial (left column) and polycrystalline (right column) series. The AFM images have the same scale (7 nm vertical and 400 nm lateral). (b) Evolution of the surface (triangles) and Fe interlayer (circles) roughness, measured by AFM and XRR, respectively, with the Fe interlayer thickness for epitaxial (full symbols) and polycrystalline (empty symbols) structures.

are shown in Fig. 2(a). It is worth noting that the AFM images are displayed with the same height and lateral scale for better comparison. As can be observed, the two samples without an Fe interlayer and the epitaxial sample with a 4.5 nm Fe interlayer exhibit a very flat surface with global differences in height of around 0.5 nm over the scanned area. On the other hand, the polycrystalline 5 nm Fe sample shows a rougher surface, including granular structures around 7 nm in height, correlated with the different buffer growth technique. In Fig. 2(b) we have plotted the Fe interlayer thickness dependence of the rms roughness of the topmost layer for both series of samples, which is systematically at least a factor of 2 larger in the polycrystalline samples than in the epitaxial ones for every Fe interlayer thickness. XRR is a very suitable tool to extract quantitative information about not only the roughness of the topmost layer in a multilayered system but also to determine the thickness and roughness of buried interfaces. The obtained results for the Fe interlayer–top Au layer interface from XRR measurements are also shown in Fig. 2(b). Although similar slope values of the Fe interlayer roughness are found in both types of structures, the same trend as that mentioned in the case of AFM results is observed. This result confirms the major role of the buffer layer morphology, which substantially affects the growth of consecutive Au, Fe, and Au layers and gives rise to systematically larger roughness for the entire multilayer. Summarizing, the epitaxial growth of the Fe interlayer and the whole layered structure for this set of samples favors the reduction of the roughness and the improvement of the overall morphology providing very smooth continuous surfaces and high-quality interfaces in terms of flatness.[40]

B. Magnetic characterization

The effect of the crystalline nature of the different magnetic properties of the two series of structures is confirmed by measuring both in-plane and out-of-plane magnetic hysteresis loops using transverse and polar Kerr effect, respectively. Figures 3 and 4 show the obtained loops for the epitaxial and polycrystalline series, respectively. In the first case, a clear in-plane fourfold anisotropy, characteristic of a (001)-oriented cubic Fe lattice is observed, as evidenced by the easy [100] and hard [110] in-plane magnetocrystalline axes shown for selected samples in the left column of Fig 3. Analyzing these magnetic measurements, we can extract a normalized remanence M_r/M_s (where M_r is the remanent magnetization and M_s is the magnetization at saturation) along the hard [110] axis. In our epitaxial series an averaged M_r/M_s value of 0.73 ± 0.02 is determined which confirms 45° between the magnetization and the magnetic field direction (i.e., the magnetization lies along the [100] direction) in the remanent state. It is worth noting that even the sample without an Fe interlayer, i.e., 14 nm Au/1 nm Fe/MgO(001), exhibits a clear in-plane anisotropy with well-defined easy and hard axes hysteresis loops. This indicates that this buffer layer has a great degree of continuity, enough to evidence the typical biaxial in-plane anisotropy of a cubic thin film. However, in the out-of-plane magnetic characterization performed by polar Kerr measurements and shown in the right column of Fig. 3, the loop of the sample with a 0 nm Fe interlayer shows a magnetic

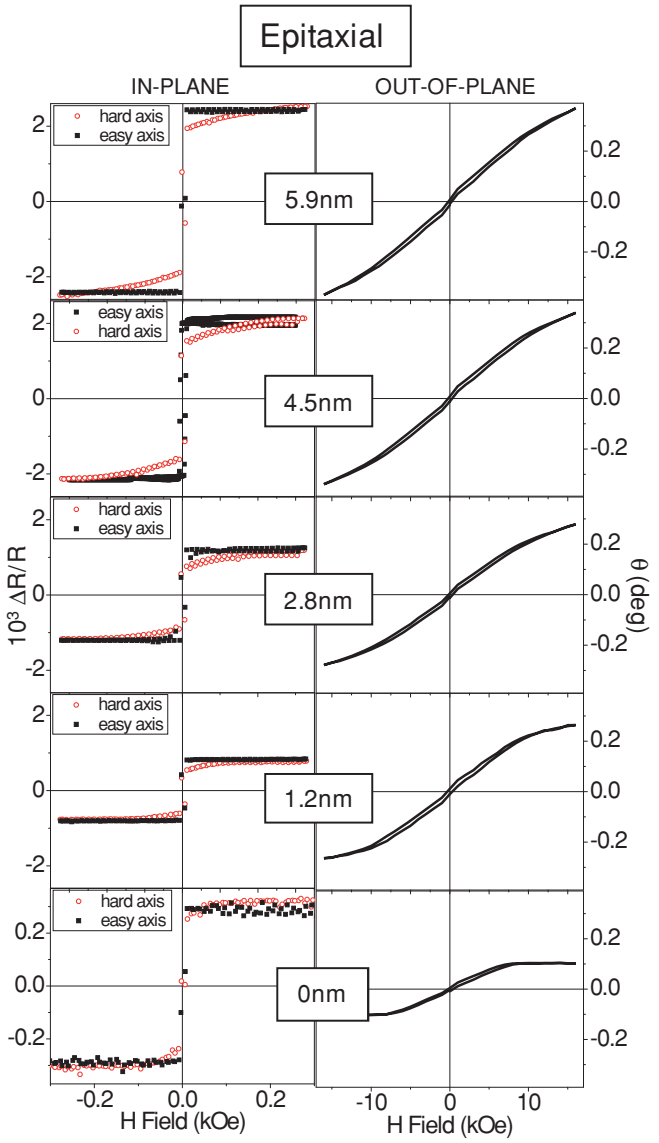

FIG. 3. (Color online) Kerr magneto-optical loops of representative epitaxial samples measured in transverse (left panel) and polar (right panel) configurations. In transverse configuration, the open and closed symbols correspond to the hard and easy magnetic axes, respectively.

saturation field of about 8 kOe, well below that expected for a continuous Fe thin film (21 kOe). This suggests that the Fe buffer film might be in the form of platelets (incomplete layer).[41] The loop of the sample with a 1.2 nm Fe interlayer exhibits a saturation field higher than 16 kOe, which indicates that the continuity of such an Fe interlayer is better than that of the buffer. Finally, for higher Fe interlayer thickness, the tendency of the loops points to the formation of continuous Fe interlayers.

On the other hand, the corresponding hysteresis loops for the polycrystalline samples are shown in Fig. 4. Rounded loops are obtained in the transverse configuration, with total absence of in-plane anisotropy (loops at 0° and 45° yield identical results), as should be expected for a polycrystalline structure, and therefore also with isotropic magnetocrystalline anisotropy. Besides, the higher in-plane coercive field for poly-

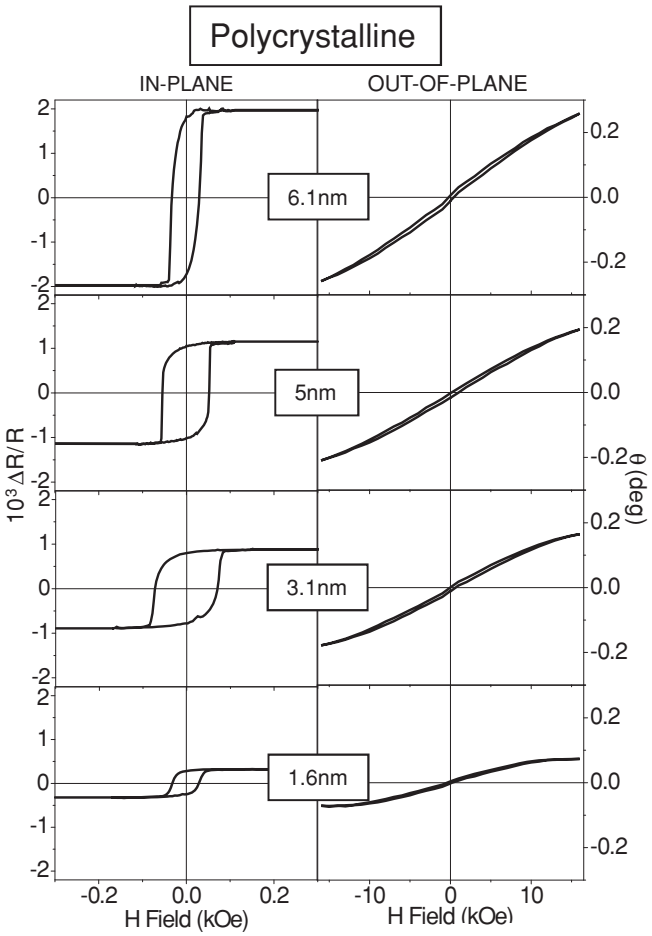

FIG. 4. Kerr magneto-optical loops of representative polycrystalline samples measured in transverse (left panel) and polar (right panel) configurations.

crystalline samples compared to the corresponding epitaxial ones (Fig. 5) can be mainly ascribed to the higher interface roughness shown in Sec. III A. Figure 5 displays the in-plane coercive field vs Fe interlayer thickness for epitaxial and polycrystalline samples. In the case of the epitaxial series it remains constant, which clearly indicates the existence of a continuous and flat Au-Fe interlayer for each Fe thickness. On the other hand, the polycrystalline series shows a coercive field increase with Fe thickness up to 3 nm Fe, probably due to an islanded morphology. At a higher Fe interlayer thickness, once coalescence forms a continuous Fe interlayer, the coercive field decreases due to an improved homogeneity. This can be attributed to a decrease in the number of pinning points for domain-wall motion when the magnetization reversal takes place.

C. Magneto-optical characterization

In order to extract the effective MO constants of the different Fe layers, polar Kerr spectra have been measured for all the samples in both series (Fig. 6). An increase of rotation (θ) and ellipticity (ϕ) is observed with Fe thickness in the two series of samples. In every spectrum, the s-shape feature found in the rotation curves (and the corresponding maxima found in the ellipticity curves) around 2.5 eV is related to the bulk-plasmon

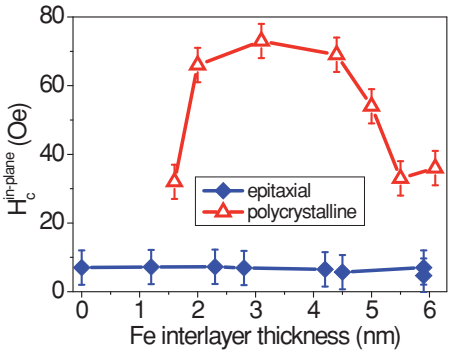

FIG. 5. (Color online) Coercive in-plane magnetic field ($H_c^{\text{in-plane}}$) vs Fe interlayer thickness for epitaxial and polycrystalline sets of samples.

resonance of Au. Interestingly, the overall MO activity of the polycrystalline samples is lower (roughly a factor of 2) than that of the equivalent epitaxial samples. Surely, we have to take into account the contribution of the 1 nm Fe buffer layer in the epitaxial series to the MO activity. However, the rotation and ellipticity spectra for the 1 nm Fe interlayer epitaxial structure (with 2 nm of total Fe thickness) exhibit an overall magnitude similar to the spectra for the 6 nm Fe polycrystalline one. This indicates that the differences between the two sets of samples do not originate simply by the presence of a MO active buffer layer on epitaxial multilayers. This reduction in the MO activity for the polycrystalline Fe layers originates from differences in the MO constants from both structures.

When analyzing the MO constants we have to take into account that there are two Fe layers in each epitaxial multilayer (except in the 0 nm Fe sample): the buffer layer and the interlayer. Therefore three representative MO constants can be extracted: the epitaxial interlayer, the epitaxial buffer (1 nm Fe), and the polycrystalline interlayer MO constants. In Fig. 7 we have plotted the MO constants corresponding to the epitaxial buffer, the 6 nm Fe epitaxial interlayer, and

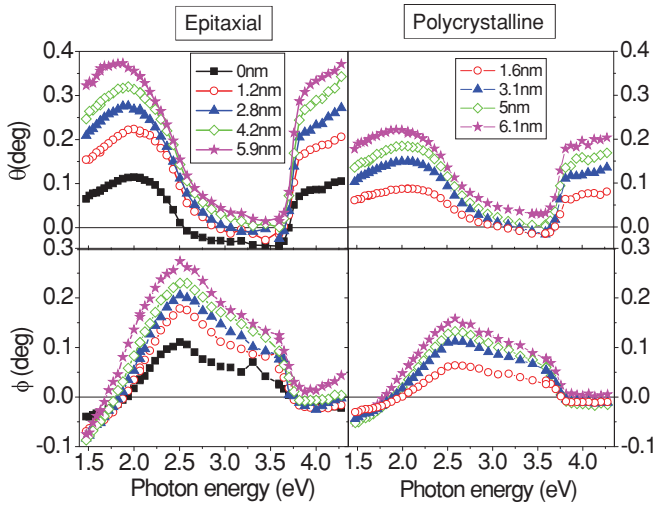

FIG. 6. (Color online) Rotation (θ) and ellipticity (ϕ) spectra of representative samples for both series of structures.

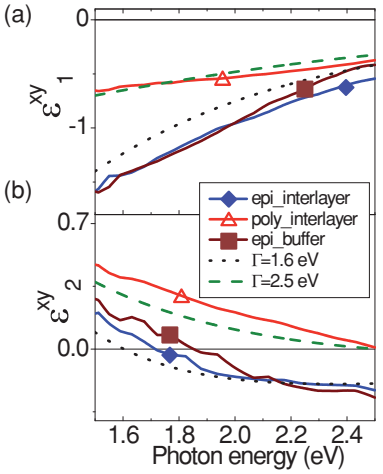

FIG. 7. (Color online) Real (a) and imaginary (b) parts of experimental magneto-optical (MO) constants for epitaxial Fe interlayer (6 nm thick), epitaxial Fe buffer layer (1 nm thick), and polycrystalline Fe interlayer (6 nm thick). In addition, two theoretical curves, using a Drude model with Γ as 1.6 and 2.5 eV (dotted and dashed curves, respectively), were added in order to compare with the experimental MO constants.

the 6 nm Fe polycrystalline interlayer. Note that no relevant differences are observed looking at the MO constants of the buffer layer and interlayer for epitaxial structures. On the other hand, the polycrystalline and epitaxial interlayers exhibit remarked differences. First, the value of the real part of the MO constants for the epitaxial interlayer is about two times larger than for the polycrystalline one at low-photon energies (1.8 times at He-Ne laser wavelength). Second, the zero crossing of the imaginary part of the MO constants for the epitaxial interlayer is located around 1.8 eV, whereas for the polycrystalline one it is located around 2.5 eV. In order to understand the origin of these relevant differences, we can use the Drude model for simulating the MO properties of the intraband contribution in an Fe layer (2). This approximation, considering only the intraband contribution, is enough to describe the MO constants in the low-photon energy region (1–5 eV), because the interband contribution on the MO activity from Fe or Co is not very important in this spectral region[42,43] and can be neglected. Therefore the MO constants are described by

$$\varepsilon_{xy}^{\text{drude}}(w) = i\frac{w_c w_p^2}{w\left[(\Gamma - iw)^2 + w_c^2\right]} \qquad (2)$$

using a value of plasma frequency of 10.2 eV, a cyclotron frequency of 0.0973 eV, and two different damping constants of 1.6 (bulk Fe) and 2.5 eV (w_p, w_c, and Γ, respectively) from Ref. 42 in this equation. The two theoretical curves corresponding to these damping constants have been plotted in Fig. 7. They exhibit good qualitative agreement with those experimentally obtained for the epitaxial and polycrystalline structures if we keep in mind that the interband contribution has not been taken into account in the theory. This points to a possible contribution to the different MO properties observed between epitaxial and polycrystalline Fe layers coming from

these different Drude damping constants (Γ) or electron-scattering times in the two kinds of metallic layers. The higher Γ obtained for the polycrystalline structure indicates a higher ratio of electronic collisions inside the polycrystalline Fe layer and at their rough interfaces as compared to the epitaxial or bulk one.[30,31]

D. Magnetoplasmonic characterization

1. Surface-plasmon resonance effects on the MO activity

Once the different structural, morphological, and MO characteristics of both series of samples are determined, the possible influences on their magnetoplasmonic properties can be studied. This has been carried out by measuring the reflectivity and transverse MO Kerr-effect (TMOKE) signal using the Kretschmann configuration[35] for a given wavelength $\lambda = 632$ nm, as sketched in Fig. 8(a).

Standard reflectivity versus incidence angle measurements as a function of the Fe interlayer thickness is shown in Fig. 8(b) for the epitaxial (left panel) and polycrystalline (right panel) structures. Focusing our attention first on the series of epitaxial samples, we can see a strong dependence on the minimum in the reflectivity as a function of the Fe interlayer thickness, with values of 0.4 for the sample without an Fe interlayer, 0.1 for the sample with a 1.2 nm Fe layer, and much lower values for the rest of the epitaxial samples. The lowest value of the reflectivity minimum is observed for the epitaxial sample with 4.5 nm Fe, since this thickness is very close to the optimum SPP excitation thickness.

With an Fe interlayer thicker than 4.5 nm, the reflectivity minimum increases because the multilayer system goes far from the optimum SPP excitation. On the other hand, this dependence is much less pronounced in the polycrystalline series, with all the minima in the reflectivity reaching values between 0.1 and 0. The lowest value reflectivity minimum is obtained for the sample of 3.1 nm Fe (optimum SPP excitation), the reflectivity minimum increasing again with thicker Fe interlayers.

Considering now the transverse Kerr signal ($\Delta R/R$) measured for both series of samples, in Fig. 8(c) we show the obtained results as a function of both the Fe interlayer thickness and the incidence angle. Remarkably, the largest $\Delta R/R$ signal values are obtained for both the epitaxial structure with the 4.5 nm Fe interlayer and the polycrystalline one with the 3.1 nm Fe interlayer. For the specific thickness of these two structures the SPP excitation is optimum, therefore exhibiting a very small (close to zero) reflectivity upon SPP excitation, and as a consequence an enhanced MO activity, which actually might diverge if values of reflectivity very close to zero were achieved. The different optimum SPP excitation thicknesses in both structures are due to the different optical absorption of the two buffer layers used, being 2 nm of Cr more absorbing than 1 nm of Fe, and consequently, a lower Fe interlayer thickness being necessary for almost optimum plasmon excitation in the polycrystalline series. It is worth noting that there is no clear influence of the crystalline nature of the structures on the plasmon excitation of the different samples.

Finally, we can represent $(\Delta R/R)_{max}$, which is the positive maximum value of TMOKE angular measurement[14,18] as a function of the Fe interlayer thickness for the two sets of

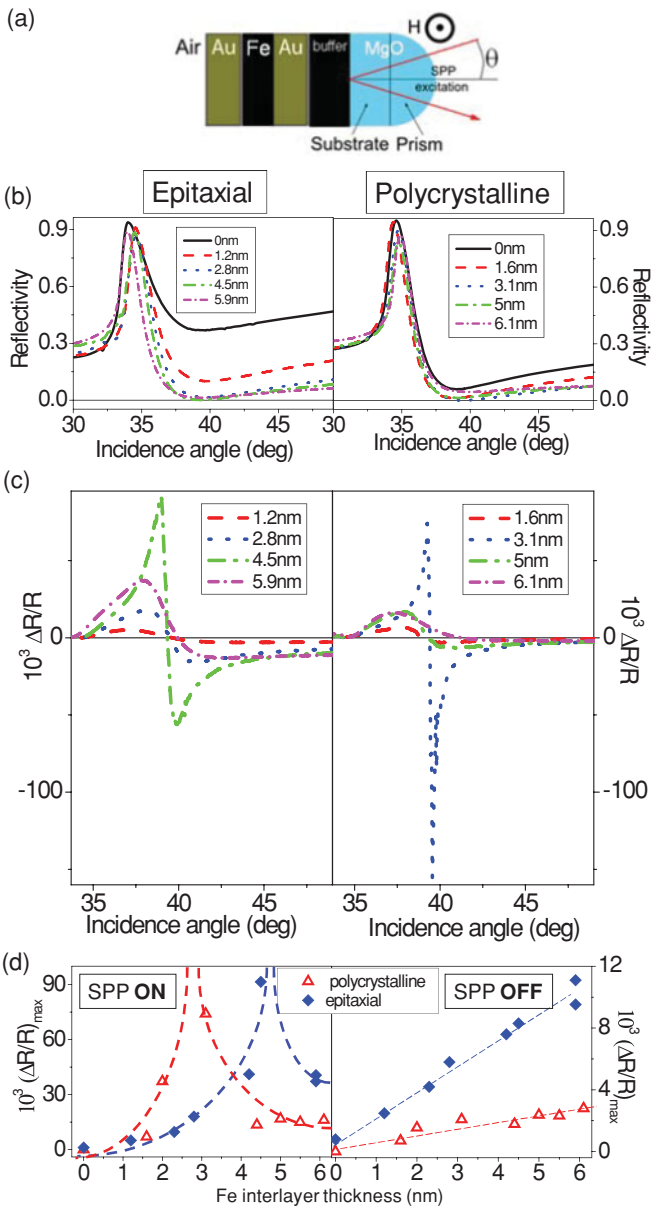

FIG. 8. (Color online) (a) Sketch of the Kretschmann configuration which allows angular measurements of the (b) reflectivity and (c) $\Delta R/R$ as a function of the Fe interlayer thickness for epitaxial (left panels) and polycrystalline (right panels) structures. (d) $(\Delta R/R)_{max}$ vs Fe interlayer thickness for both polycrystalline (red triangles) and epitaxial (blue diamonds) samples, with (left panel) and without (right panel) SPP excitation. Dashed lines are guides for the eyes. Notice the different vertical scales when comparing the left and right panels.

samples with and without SPP excitation [see Fig. 8(d)]. When SPP is excited [left panel of Fig. 8(d)], the $(\Delta R/R)_{max}$ exhibits a maximum at the mentioned optimum SPP thickness for polycrystalline and epitaxial structures (3.1 and 4.5 nm Fe thickness, respectively), decreasing for thicker Fe layers. In contrast, when no SPP is excited [right panel of Fig. 8(d)] $(\Delta R/R)_{max}$ shows a typical monotonous increase with Fe amount for both sets of samples. The influence of the higher MO constants of the epitaxial samples with respect to the polycrystalline ones is clearly observed, with the higher

TMOKE signal increase with Fe amount for the epitaxial structures compared to that for the polycrystalline ones (a factor of 3).

In summary, the very large $\Delta R/R$ ratios with SPP excitation obtained in the polycrystalline and epitaxial systems at different Fe interlayer thicknesses (3.1 and 4.5 nm, respectively) are simply due to the proper thickness obtained in these two samples for optimum plasmon excitation, being the different Fe interlayer thickness attributed to the different absorption of Cr and Fe buffer layers. On the other hand, the $\Delta R/R$ signal without SPP excitation is directly related to the MO constants of both series of samples following the same trend but exhibiting a larger linear increase for the epitaxial multilayers.

2. *Magnetic modulation of the SPP resonance*

Another issue of interest is the potential use of these magnetoplasmonic structures in active plasmonic devices. The ferromagnetic layer in the multilayered structure introduces sizable off-diagonal components in the dielectric tensor of the whole system. Thus the application of a low external magnetic field can produce a modulation in the wave vector of the SPP. This SPP modulation has been reported in previous works using Co as the ferromagnetic layer.[14,18,19,22] Here we have measured this effect in both epitaxial and polycrystalline structures with Fe as the ferromagnetic layer.

With the measurements shown in Sec. III D 1, and following the formalism detailed in Refs. 14 and 18, based on the comparison between the angular derivative of the reflectivity and the angular dependence of $\Delta R/R$, the magnetic-field-induced modulation of the SPP wave vector can be determined. In Fig. 9, using symbols we present the experimentally obtained modulation as a function of the Fe interlayer thickness for both epitaxial and polycrystalline structures. As can be seen, $\Delta k/k$ increases with Fe interlayer thickness for both series of samples, with systematically larger values for the epitaxial samples, especially for Fe thicknesses above 2.5 nm, whereas the observed modulation is similar for both series below this value. Obviously, the nonzero wave vector modulation obtained for the epitaxial sample without a Fe interlayer is due to the effect of the Fe buffer layer, whereas in the polycrystalline series the Cr buffer does not contribute to the modulation since Cr is not ferromagnetic.

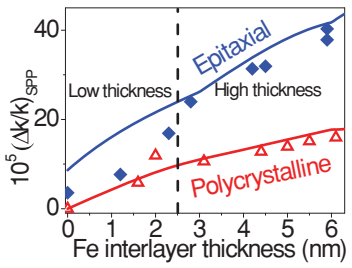

FIG. 9. (Color online) Fe interlayer dependence of experimentally (symbols) and simulated (continuous lines) $(\Delta k/k)_{SPP}$ using the actual MO constants obtained from epitaxial (diamonds) and polycrystalline (triangles) sets of structures.

To understand the observed differences, the modulation of the SPP wave vector as a function of the Fe interlayer thickness has been calculated using the transfer-matrix formalism,[44] assuming sharp interfaces between the different layers and using the effective MO constants experimentally determined by polar Kerr spectroscopy (see Sec. III C)[18] for the 6 nm Fe epitaxial and polycrystalline interlayer samples. Note that the effective magneto-optical constant of the Fe layer is roughly a factor of 2 lower in the polycrystalline sample than in the epitaxial one for the considered wavelength. The calculated results are shown in Fig. 9 as continuous lines, with very good agreement with the experimental data corresponding to both series of samples with the only exception being the epitaxial samples having Fe interlayer thicknesses below 2.5 nm.

This observed difference in $\Delta k/k$ is therefore ascribable to the reduced effective MO constants of the Fe interlayer for the polycrystalline series with respect to the epitaxial one. This reduction of the effective Fe MO constants can be interpreted in two ways: either because a system with a rough interface can be optically considered as an effective medium composed by Fe and Au, and therefore with effective MO constants lower than those of bulk Fe, or just by a purely interfacial effect where the MO constants of the Fe atoms at the Fe-Au interface are smaller from bulk Fe due to hybridization effects,[33] and are therefore proportional to the interface area, which will be larger for a system with rough interfaces. On the other hand, the deviation from the expected trend in the epitaxial series for Fe thickness below 2.5 nm (mainly for the 1.2 nm Fe sample) can be understood from the lack of completeness of the Fe interlayer at this thickness range as discussed in Sec. III B. This lack of completeness gives rise to a region where Fe and Au coexist, and therefore can be considered as a layer with effective MO constants lower than those of bulk Fe.

IV. CONCLUSIONS

We have carried out a systematic study comparing the structural, morphological, magnetic, MO, and magnetoplasmonic properties of epitaxial and polycrystalline Au/Fe/Au trilayers as a function of the Fe interlayer thickness. We find a direct effect of the higher crystalline and interface quality of the epitaxial structures on the MO constants of Fe, which as a consequence gives rise to an increase in the MO activity (threefold) and in the magnetic modulation of the SPP wave vector (twofold) with respect to their equivalent polycrystalline ones. On the other hand, the MO activity with SPP excitation mainly depends on the achievement of the exact layer thickness that leads to optimum plasmon excitation, and as a consequence, to a minimum in the reflectivity and a maximum in the TMOKE signal. This work demonstrates the crucial role that crystallinity and interface sharpness play on the optimization of the MO and magnetoplasmonic properties of noble metal-ferromagnetic heterostructures.

ACKNOWLEDGMENTS

Financial support from the Spanish MICINN (Grants No. MAT2008-06765-C02-01/NAN, No. MAT2007-66719-C03, No. MAT2010-18432, No. NAN2004-09195-C04-02, and No. CSD2008-00023), Comunidad de Madrid (Grants

No. S2009/TIC-1476, No. S2009/MAT-1726, and No. S-0505/TIC/0191), CSIC (JAE fellowship for E.F.-V.), and European Commission (Grant No. NMP3-SL-2008-214107) is acknowledged.

[1]H. Raether, *Surface Plasmons on Smooth and Rough Surfaces and on Gratings*, Springer Tracts in Modern Physics Vol. 111 (Springer-Verlag, Berlin, 1988).
[2]S. I. Bozhevolnyi, V. S. Volkov, E. Devaux, J. Y. Laluet, and T. W. Ebbesen, Nature (London) **440**, 508 (2006).
[3]B. Steinberger, A. Hohenau, H. Ditlbacher, A. L. Stepanov, A. Drezet, F. R. Aussenegg, A. Leitner, and J. R. Krenn, Appl. Phys. Lett. **88**, 094104 (2006).
[4]J.-C. Weeber, Y. Lacroute, and A. Dereux, Phys. Rev. B **68**, 115401 (2003).
[5]Z. Liu, S. Durant, H. Lee, Y. Pikus, N. Fang, Y. Xiong, C. Sun, and X. Zhang, Nano Lett. **7**, 403 (2007).
[6]I. I. Smolyaninov, J. Elliott, A. V. Zayats, and C. C. Davis, Phys. Rev. Lett. **94**, 057401 (2005).
[7]J. Homola, Chem. Rev. **108**, 462 (2008).
[8]B. Sepúlveda, A. Calle, L. M. Lechuga, and G. Armelles, Opt. Lett. **31**, 1085 (2006).
[9]D. Pacifici, H. J. Lezec, and H. A. Atwater, Nat. Photonics **1**, 402 (2007).
[10]T. Nikolajsen, K. Leosson, and S. I. Bozhevolnyi, Appl. Phys. Lett. **85**, 5833 (2004).
[11]M. J. Dicken, L. A. Sweatlock, D. Pacifici, H. J. Lezec, K. Bhattacharya, and H. A. Atwater, Nano Lett. **8**, 4048 (2008).
[12]V. I. Safarov, V. A. Kosobukin, C. Hermann, G. Lampel, J. Peretti, and C. Marlière, Phys. Rev. Lett. **73**, 3584 (1994).
[13]C. Hermann, V. A. Kosobukin, G. Lampel, J. Peretti, V. I. Safarov, and P. Bertrand, Phys. Rev. B **64**, 235422 (2001).
[14]J. B. González-Díaz, A. García-Martín, G. Armelles, J. M. García-Martín, C. Clavero, A. Cebollada, R. A. Lukaszew, J. R. Skuza, D. P. Kumah, and R. Clarke, Phys. Rev. B **76**, 153402 (2007).
[15]E. Ferreiro-Vila, X. M. Bendana Sueiro, J. B. Gonzalez-Diaz, A. García-Martin, J. M. García-Martin, A. Cebollada Navarro, G. Armelles Reig, D. Meneses Rodriguez, and E. Munoz Sandoval, IEEE Trans. Magn. **44**, 3303 (2008).
[16]G. Armelles, J. B. González-Díaz, A. García-Martín, J. M. García-Martín, A. Cebollada, M. U. González, S. Acimovic, J. Cesario, R. Quidant, and G. Badenes, Opt. Express **16**, 16104 (2008).
[17]L. Sapienza and D. Zerulla, Phys. Rev. B **79**, 033407 (2009).
[18]E. Ferreiro-Vila, J. B. González-Díaz, R. Fermento, M. U. González, A. García-Martín, J. M. García-Martín, A. Cebollada, and G. Armelles, Phys. Rev. B **80**, 125132 (2009).
[19]V. V. Temnov, G. Armelles, U. Woggon, D. Guzatov, A. Cebollada, A. García-Martin, J.-M. García-Martin, T. Thomay, A. Leitenstorfer, and R. Bratschitsch, Nat. Photonics **4**, 107 (2010).
[20]C. Clavero, K. Yang, J. R. Skuza, and R. A. Lukaszew, Opt. Express **18**, 7743 (2010).
[21]C. Clavero, K. Yang, J. R. Skuza, and R. A. Lukaszew, Opt. Lett. **35**, 1557 (2010).
[22]D. Martín-Becerra, J. B. González-Díaz, V. V. Temnov, A. Cebollada, G. Armelles, T. Thomay, A. Leitenstorfer, R. Bratschitsch, A. García-Martín and M. U. González, Appl. Phys. Lett. **97**, 183114 (2010).
[23]P. Nagpal, N. C. Lindquist, S.-H. Oh, and D. J. Norris, Science **325**, 594 (2009).
[24]X. Zhu, Y. Zhang, J. Zhang, J. Xu, Y. Ma, Z. Li, and D. Yu, Adv. Mater. **22**, 4345–4349 (2010).
[25]V. Krishan and R. H. Ritchie, Phys. Rev. Lett. **24**, 1117 (1970).
[26]M. Kuttge, E. J. R. Vesseur, J. Verhoeven, H. J. Lezec, H. A. Atwater, and A. Polman, Appl. Phys. Lett. **93**, 113110 (2008).
[27]K.-P. Chen, V. P. Drachev, J. D. Borneman, A. V. Kildishev, and V. M. Shalaev, Nano Lett. **10**, 916 (2010).
[28]Y. Saito, J. J. Wang, D. N. Batchelder and D. A. Smith, Langmuir **19**, 6857 (2003).
[29]M. Grzelczak, B. Rodríguez-González, J. Pérez-Juste, and L. M. Liz-Marzán, Adv. Mater. **19**, 2262 (2007).
[30]C. Clavero, B. Sepúlveda, G. Armelles, Z. Konstantinovic, M. García del Muro, A. Labarta, and X. Batlle, J. Appl. Phys. **100**, 074320 (2006).
[31]C. Clavero, A. Cebollada, G. Armelles, Y. Huttel, J. Arbiol, F. Peiró, and A. Cornet, Phys. Rev. B **72**, 024441 (2005).
[32]A. A. Sidorenko, C. Pernechele, P. Lupo, M. Ghidini, M. Solzi, R. De Renzi, I. Bergenti, P. Graziosi, V. Dediu, L. Hueso, and A. T. Hindmarch, Appl. Phys. Lett. **97**, 162509 (2010).
[33]L. Uba, S. Uba, V. N. Antonov, A. N. Yaresko, T. Śzak, and J. Koreck, Phys. Rev. B **62**, 13731 (2000).
[34]D. Regatos, D. Fariña, A. Calle, A. Cebollada, B. Sepúlveda, G. Armelles, and L. M. Lechuga, J. Appl. Phys. **108**, 054502 (2010).
[35]E. Kretschmann and H. Raether, Z. Naturforsch. A **23**, 2135 (1968); E. Kretschmann, Z. Phys. **241**, 313 (1971).
[36]W. S. Kim, M. Aderholz, and W. Kleemann, Meas. Sci. Technol. **4**, 1275 (1993).
[37]C. Martínez Boubeta, A. Cebollada, J. F. Calleja, C. Contreras, F. Peiró, and A. Cornet, J. Appl. Phys. **93**, 2126 (2003).
[38]A. Singh, V. Neu, R. Tamm, K. Subba Rao, S. Fähler, W. Skrotzki, L. Schultz, and B. Holzapfe, Appl. Phys. Lett. **87**, 072505 (2005).
[39]J. Shen, Z. Gaib, and J. Kirschner, Surf. Sci. Reports **52**, 163 (2004).
[40]E. Paz, F. Cebollada, F. J. Palomares, F. García-Sánchez, and J. M. González, Nanotechnology **21**, 255301 (2010).
[41]C. Martínez Boubeta, C. Clavero, J. M. García-Martín, G. Armelles, A. Cebollada, Ll. Balcells, J. L. Menéndez, F. Peiró, A. Cornet, and M. F. Toney, Phys. Rev. B **71**, 014407 (2005).
[42]G. S. Krinchik, J. Appl. Phys. **35**, 1089 (1964).
[43]R. Carey and B. W. J. Thomas, J. Phys. D: Appl. Phys. **7**, 2362 (1974).
[44]M. Schubert, Phys. Rev. B **53**, 4265 (1996).